From ferromagnetic to helical order with a discussion of the low-temperature antiferromagnetism in composite $Cd_{1-x}Mn_xGeP_2$+MnP semiconductors

L. Kilanski [ORCID],[1,*] S. Lewińska [ORCID],[1] A. Khaliq,[1] R. Minikaev,[1] A. Reszka,[1] A. Ślawska-Waniewska,[1]
B. J. Kowalski [ORCID],[1] T. R. Arslanov [ORCID],[2,†] and S. F. Marenkin[3]

[1]*Institute of Physics, Polish Academy of Sciences, Aleja Lotnikow 32/46, PL-02668 Warsaw, Poland*
[2]*Amirkhanov Institute of Physics, Daghestan Federal Research Center, RAS, 367003 Makhachkala, Russia*
[3]*Kurnakov Institute of General and Inorganic Chemistry, RAS, 119991 Moscow, Russia*
and National University of Science and Technology, 119049 Moscow, Russia

Mn-doped chalcopyrites exhibit rich and unique physical properties due to the presence of magnetic clusters, both at ambient and under high external pressures. Despite recent efforts and rich literature on this topic, it is still necessary to explain some of the phenomena occurring in these systems, such as the origin of magnetic interactions at ambient pressure. In this context, we report the investigations of physical mechanisms responsible for the magnetic order of a $Cd_{1-x}Mn_xGeP_2$+MnP composite system with changeable Mn contents x, ranging from 0.008 to 0.037. The presence of MnP clusters, confirmed by energy dispersive x-ray spectrometry and scanning electron microscopy methods, is responsible for the ferromagnetic phase transition with the Curie temperature T_C around 295 K. Moreover, the transition from ferromagnetic to helical order is observed, with the critical temperature T_S changing from 78 K for the sample with $x = 0.008$ down to 54 K for $x = 0.037$. Besides the common explanation based on the structural disorder at the cluster surface and finite-size effects, we associate the observed $T_S(x)$ dependence with the local pressure effect due to Mn doping, where the influence of the external pressure $P \sim 0.25$ GPa corresponds to the influence of the Mn content $x = 0.035$.

I. INTRODUCTION

Complex ferromagnetic semiconductors (FMSs) are a very important group of materials with promising properties for spintronics. These semiconductors offer numerous benefits over intensively studied and well-known Mn-doped III-V, II-VI, and IV-VI semiconductors [1–4]. Among several important uses of FMSs as spin injection and spin current detection materials is their functionality in spin devices at room temperature. Unfortunately, a few decades of improvement in the ferromagnetic properties of III-V and IV-VI FMSs allowed increasing the Curie temperature T_C only up to values not exceeding 200 K in $Ga_{1-x}Mn_xAs$ based compounds [5–10]. In this regard, the lack of homogeneous FMSs possessing room-temperature ferromagnetism is garnering increasing attention to investigate nanocomposite systems, consisting of high-T_C ferromagnetic clusters implanted into the semiconductor matrix.

Complex FMS systems based on chalcopyrite II-IV-V$_2$ semiconductors have attracted large scientific interest due to the observation of ferromagnetism above room temperature [11–15]. In several II-IV-V$_2$ FMSs such as ZnGeAs$_2$:MnAs [16] and CdGeAs$_2$ + MnAs [17], the magnetic clusters present in the structure lead to a domination of short-range magnetic interactions in the system, which in turn, are respon-

sible for the room-temperature ferromagnetic order. Among Mn-doped II-IV-V$_2$ alloys, the presence of self-organized nanoclusters was recently achieved [18]. Perhaps it will allow gaining control over the structural properties of II-IV-V$_2$-based nanocomposites. This in turn should allow gaining control of the mutual influence between the structural, magnetic, and electrical phenomena of the system. Specifically, it is imperative from the point of view of potential applications to gain control over structural and magnetic properties which is necessary to control the giant magnetoresistive phenomena observed in several II-IV-V$_2$ FMSs [19].

It is known that a direct relationship between magnetic and structural properties of condensed matter can be successfully probed by means of chemical doping or application of high pressure. Undoubtedly, the pressure has a significant advantage since it provides efficient and precisely controlled changes in the volume parameters of the substance. In recent years, high-pressure magnetic and transport studies of the Mn-doped II-IV-V$_2$ semiconductors have shown a number of unusual phenomena, including the anomalous magnetization hysteresis [20], and an interesting type of "structure-driven" magnetoresistance [21]. These properties have not been seen at ambient pressure and are generally related to peculiar physics of MnP or MnAs inclusions in a semiconductor host.

In general, the origin of magnetic interactions in nanoscale and micron-size clusters should be similar to their bulk analogs, but for Mn-doped CdGeP$_2$—the first known chalcopyrite FMS [22]—the magnetic phase diagram demonstrates certain differences compared to that of bulk MnP.

*kilan@ifpan.edu.pl
†arslanovt@gmail.com

The magnetic field–pressure phase diagram of the MnP clusters in the $CdGeP_2$ matrix proposed in [20] does not exhibit a signature of the Lifshitz point, like that in bulk MnP [23]. Furthermore, the structural transition (related to $CdGeP_2$ decomposition into NaCl-type structure) resulting in a paramagnetic-ferromagnetic phase transition of MnP clusters can be either pressure induced at room temperature or temperature induced at ambient pressure [24], while the ferromagnetic phase below $T_C = 291$ K in the bulk MnP is gradually suppressed with increasing pressure [25], and disappears entirely at 3.8 GPa [26]. Seemingly, these differences arise from the cluster features related to structural distortions of MnP due to the surrounding matrix, surface, and finite-size effects. In chalcopyrite materials, formation of the MnP clusters occurs naturally as a consequence of phase segregation [27] and, therefore, it should strongly depend on the Mn content level. However, detailed studies and explanation of the separation processes and their influence on the magnetic properties are still scarce, especially for Mn-doped $CdGeP_2$ in the low-temperature range [28].

The present paper extends our previous high-pressure magnetic studies of $Cd_{1-x}Mn_xGeP_2$+MnP crystals performed at room temperature [20,24] in which temperature-dependent measurements were made. In this work, we undertake the studies of $Cd_{1-x}Mn_xGeP_2$ samples with average Mn content x, changing from 0.008 up to 0.037. We have explored structural and magnetic properties of $Cd_{1-x}Mn_xGeP_2$+MnP samples including (i) the possibility of random distribution of Mn ions in $CdGeP_2$ lattice and (ii) the clustering of Mn ions into MnP magnetic clusters. In all the cases, we observed the strong signature of MnP clusters, which was confirmed by dynamic magnetic susceptibility and static magnetization measurements as a function of the magnetic field and temperature. The comparison of the influence of Mn doping and pressure on the chalcopyrite lattice is also presented and summarized in the *T-P* phase diagram together with the literature data for bulk MnP.

II. SAMPLE PREPARATION

For the purposes of the current research, a series of $Cd_{1-x}Mn_xGeP_2$+MnP crystals were grown with the use of the direct fusion method. The growth procedure used for the preparation of our samples is similar to the one presented by Novotortsev *et al.* [29]. The synthesis of the samples was done using a high-purity CdP_2 and Ge powders milled from single crystals as starting materials. High-purity grade Mn was also used for the growth procedure. The chemical composition of the synthesized alloys was selected to stay along the hypothetical $CdGeP_2$-$MnGeP_2$ line on the phase diagram requiring the correct weights of the starting elements and preserving the correct stoichiometry of the alloy. The purity of the starting materials was high with impurity content lower than 10^{-5} wt %. The synthesis of the samples was performed using a nongradient resistance furnace equipped with a single-zone heater without temperature gradient and with controllable temperature monitored by a thermocouple sensor. The synthesis started from sealing the starting materials in quartz ampoules (sealed and pumped down to the pressure $p < 10^{-6}$ mbar), then temperature was increased to 450 °C.

The synthesis temperature was settled and stabilized for about 48 h in order to homogenize the melted synthesis constituents. After 48 h, the temperature was increased up to 800 °C at a speed of no more than 5 °C/h, and the sample was kept at 800 °C for 24 h. The sample synthesis ended with the ampoule quenched to the room temperature at a speed of 5 °C–10 °C/s.

III. STRUCTURAL CHARACTERIZATION

The chemical composition of the as-grown crystals was determined with the use of the energy dispersive x-ray fluorescence method (EDXRF). The chemical content studies were performed using the Tracor X-ray Spectrace 5000 EDXRF spectrometer. The as-grown ingots were cut into thin slices (with thickness typically around 1 mm) perpendicular to the growth direction with the use of a precision wire saw. The maximum relative errors of the EDXRF technique do not exceed 10% of the calculated value of the Mn content x. The results of the EDXRF measurements are gathered in Table I.

The performed EDXRF studies allowed us to calculate molar fractions of the elements present in the $Cd_{1-x}Mn_xGeP_2$ alloy. Within the limits of accuracy of the EDXRF spectrometer, our samples show right stoichiometry of the $Cd_{1-x}Mn_xGeP_2$ solid solution equal to 1-x:x:1:2. Correct stoichiometry of our samples allowed us to calculate the average Mn content x for each sample. The calculated x values change in the range from 0 to 0.037.

The structural quality of our samples was determined using the high-resolution x-ray diffractometer (HRXRD). The HRXRD measurements were done for all of the $Cd_{1-x}Mn_xGeP_2$ crystals at room temperature. Measurements were done with the use of multipurpose X'Pert PRO MPD, Panalytical diffractometer with Cu $K\alpha_1$ radiation with wavelength $\lambda = 1.5406$ Å, configured for Bragg-Brentano diffraction geometry and equipped with an incident-beam Johansson monochromator and a strip detector. In order to increase the quality and the accuracy of the obtained diffraction patterns, the data acquisition in each individual measurement was performed for about 3 h in the 5°–140° 2θ range. Owing to the high sensitivity of the diffractometer used, the patterns with low intensity of about 0.15% of the overall count rate can be identified. The HRXRD patterns obtained for all of our samples were analyzed with the use of the Rietveld refinement method. The data analysis showed that all our samples are inhomogeneous. The exemplary HRXRD patterns with reflections assigned to each of the detected phases marked are presented in Fig. 1.

Three different phases can be observed for the $Cd_{1-x}Mn_xGeP_2$ sample with $x = 0$, while for the samples with $x > 0$ only two phases are observed. The data analysis indicates that the main crystallographic phase of all our samples is chalcopyrite tetragonal type (*I*-42*d* group of symmetry). The calculated values of the lattice parameters, a_1 and c_1, for our samples are gathered in Table I and are close to the database data for the tetragonal $CdGeP_2$ phase with lattice parameters $a_1 = 5.7380$ Å and $c_1 = 10.7650$ Å [JCPDS, 41-1291]. In addition, we identified the presence of the cubic Ge phase (*Fd*3*m* symmetry) with lattice parameter $a_2 = 2.9793$ Å [JCPDS, 04-0545], and the hexagonal Cd phase (*P*63/*mmc* symmetry) with lattice parameters similar to

TABLE I. Results of a basic structural characterization of the $Cd_{1-x}Mn_xGeP_2$+MnP crystals including the average chemical composition x, obtained with the use of the EDXRF method and the results of the HRXRD data refinement including the lattice parameters a_1 and c_1; and the volume of the tetragonal chalcopyrite unit cell V_1 obtained for the chalcopyrite $CdGeP_2$ phase, the lattice parameter a_2, and fraction percentage P_2, for the cubic Ge phase, and the lattice parameters a_3 and c_3, and fraction percentage P_3, for the hexagonal Cd phase.

	CdGeP$_2$ (I-42d)			Ge (Fd3m)		Cd (P63/mmc)		
$x \pm \Delta x$	a_1 (Å)	c_1 (Å)	V_1 (Å)	a_2 (Å)	P_2 (%)	a_3 (Å)	c_3 (Å)	P_3 (%)
0.0	5.73658(6)	10.7940(2)	355.21	5.6240(2)	5.3(1)	2.9798(1)	5.6195(4)	1.9(1)
0.008 ± 0.001	5.73841(3)	10.7794(1)	354.96	5.6362(1)	2.4(2)	–	–	–
0.016 ± 0.001	5.74029(2)	10.76811(6)	354.81	5.65778(5)	10.9(2)	–	–	–
0.023 ± 0.002	5.73887(2)	10.76565(6)	354.56	5.6569(2)	1.0(1)	–	–	–
0.037 ± 0.002	5.73814(2)	10.764408(6)	354.43	5.65759(6)	2.5(1)	–	–	–

the database data $a_3 = 2.9793$ Å and $c_3 = 5.6181$ Å [JCPDS, 05-0674]. The lattice parameter values obtained for all our samples are gathered in Table I. The obtained lattice parameter values for all observed phases in our samples have values close to the known literature data. It should be emphasized that we found no evidence for any crystallographic phase related to Mn. It might indicate that either the Mn clustering is not present in our samples or possibly Mn-related clusters have sizes well below a micrometer that makes them hard to detect with the HRXRD technique. It is also possible that Mn-related clusters are amorphous, thus being undetectable for the HRXRD technique.

The microscopic structural properties of our $Cd_{1-x}Mn_xGeP_2$+MnP crystals were studied with the use of the Hitachi SU-70 Analytical Ultra-High-Resolution Scanning Electron Microscope (SEM) coupled with a Thermo Fisher NSS energy dispersive x-ray spectrometer

(EDS) equipped with a silicon drift detector type. All our $Cd_{1-x}Mn_xGeP_2$+MnP samples having different chemical compositions were polished and cleaned before the SEM/EDS measurements. We obtained a series of high-resolution crystal surface images measured at different sample spots and using different magnifications. The SEM measurements reveal the presence of micrometer-size inhomogeneities in all of our samples [see Fig. 2(a)].

The presence of the MnP clusters detected by the SEM measurements should be clearly visible in Fig. 2. The detailed SEM measurements reveal that for each of our samples, MnP clusters with NiAs-type hexagonal structure are observed, distributed randomly in the $Cd_{1-x}Mn_xGeP_2$+MnP lattice. At first glance, this result is in contradiction with the HRXRD results, which do not show the presence of clusters associated with manganese ions. It is therefore possible that these precipitations do not have a well-defined crystal structure, possibly are amorphous, or consist of very small crystallites. The detailed EDS measurements performed for the selected spots of the sample surfaces (selected EDS spectra presented on the right part of Fig. 2) indicate that the chemical content of the Mn-related clusters points to the possible presence of MnP clusters in our samples. The size of the clusters has very broad distribution ranging from 10 μm up to about 30 μm. The EDS data taken from sample spots where the host $Cd_{1-x}Mn_xGeP_2$+MnP lattice is observed show correct stoichiometry of the alloy and the presence of a small amount of Mn (not exceeding $x \approx 0.01$), presumably randomly distributed in the semiconductor lattice. It is a signature that the solubility of Mn in the $CdGeP_2$ crystal lattice is around 1 mol%. Ge precipitates observed during the HRXRD studies for our samples with $x > 0$ may be related to the presence of Mn randomly distributed in the $CdGeP_2$ lattice, leading to excess metal melt and phase separation. It should be noted that the technological processes were done in a way to compensate the addition of Mn to the alloy.

IV. MAGNETIC PROPERTIES

The magnetic characterization of our $Cd_{1-x}Mn_xGeP_2$+MnP samples was carried out using three magnetometers: a LakeShore 7229 AC Susceptometer/DC Magnetometer system, an Oxford Instruments vibrating sample magnetometer (VSM) system, and a Quantum Design XL-5 magnetic property measurement system. The first system allows us to measure the dynamic magnetic susceptibility χ_{AC} and the
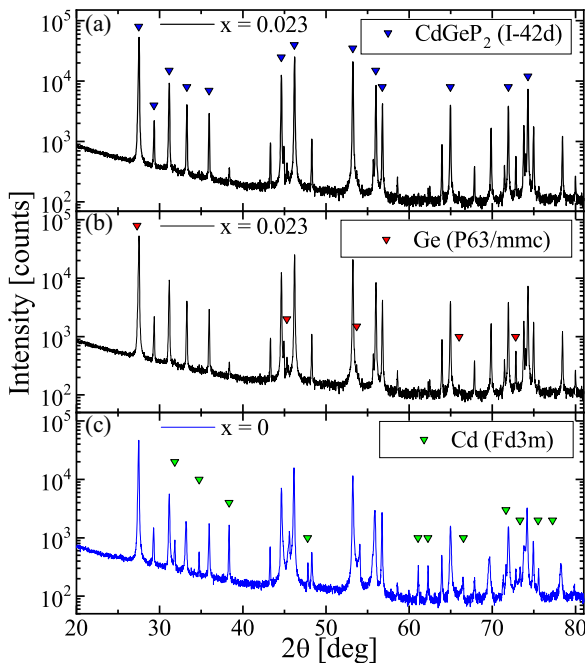

FIG. 1. Results of the HRXRD measurements obtained at room temperature for the exemplary $Cd_{1-x}Mn_xGeP_2$+MnP samples with $x = 0$ and $x = 0.023$ showing three detected phases in these alloys including (a) chalcopyrite $CdGeP_2$, (b) cubic Ge, and (c) hexagonal Cd phases.
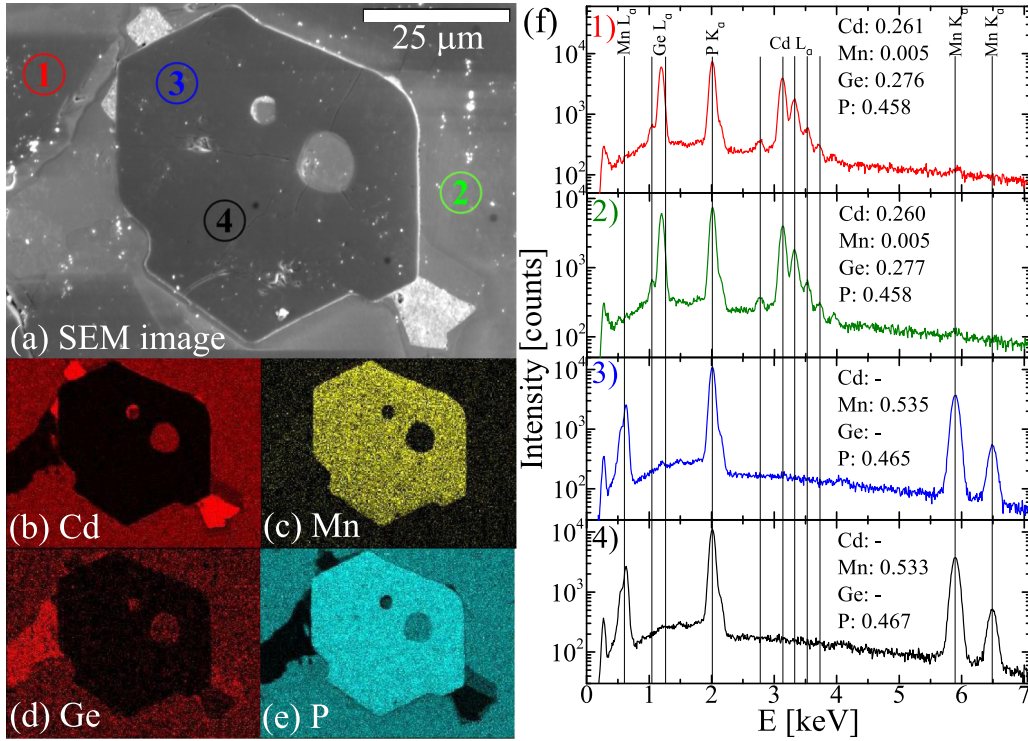
FIG. 2. Results of the SEM/EDS measurements obtained at room temperature for the exemplary $Cd_{1-x}Mn_xGeP_2$+MnP sample with $x = 0.012$ including (a) SEM image and [(b)–(f)] EDX microprobe results including (b)–(e) maps of the distribution of the alloying elements and (f) the detailed chemical content measurement executed at different spots [marked as numbers in Fig. 2(a)] of the sample surface.

high-field static magnetization M as a function of the magnetic field B. The temperature-dependent magnetization measurements in the low-field regime were done using the latter two measuring systems.

At first, the detailed measurements of χ_{AC} were performed at temperatures ranging from 4.3 K up to a maximum of about 320 K for an exciting field of 1 mT and a frequency $f = 625$ Hz. The contribution of the sample holder was subtracted from the experimental data. Accordingly, we obtained the temperature dependencies of complex susceptibility, namely, real, $Re(\chi_{AC})$, and imaginary, $Im(\chi_{AC})$ parts of the magnetic susceptibility. A vanishing $Im(\chi_{AC})$ part was registered for all of our $Cd_{1-x}Mn_xGeP_2$+MnP crystals; thus in Fig. 3 only the temperature dependencies of the real part of the AC magnetic susceptibility are presented. At temperatures $T \leqslant 320$ K, the $Re(\chi_{AC})(T)$ curves display positive values which change significantly with temperature. As visible in Fig. 3, a rapid decrease of the magnetic susceptibility with heating from 280 to 310 K is related to the ferromagnetic phase transition in the investigated samples, described for MnP systems (T_C near 290 K) in the literature earlier [30,31]. Most probably, the MnP clusters embedded in the $Cd_{1-x}Mn_xGeP_2$+MnP lattice are a source of such behavior. The estimated T_C values for all samples, as a point where $\partial^2 Re(\chi_{AC})/\partial T^2 = 0$, are listed in Table II. Besides the similarity of the obtained T_C values (from 292 to 295 K) to those reported in [30–33] Curie temperatures for MnP single crystals equal to 291 K [30–33], it should be highlighted that our II-IV-V$_2$ samples are ternary equivalents of the binary III-V compound of GaP with MnP clusters, for which similar magnetic behavior near $T = 300$ K is observed [34].

At temperatures lower than 50 K, an increase of $Re(\chi_{AC})$ with a temperature decrease is observed, indicating the presence of a paramagnetic component, which dominates the magnetic susceptibility related to the MnP clusters. It is therefore probable that this paramagnetic component comes from manganese ions incorporated into the $CdGeP_2$ host lattice
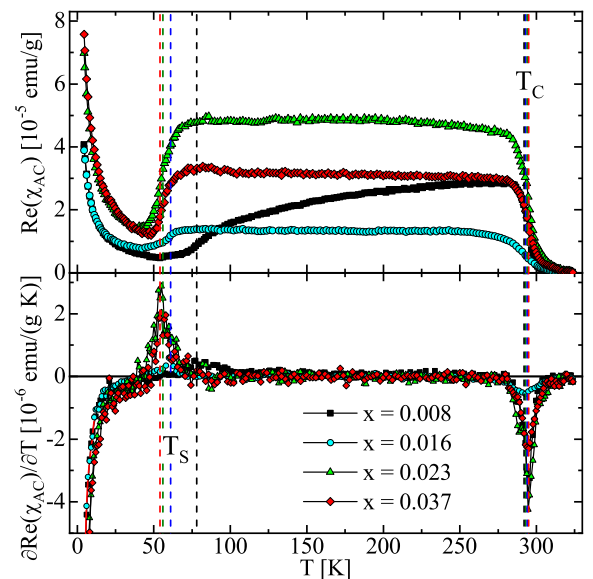

FIG. 3. Temperature dependence of the AC magnetic susceptibility (top figure) and its derivative (bottom figure) obtained for the $Cd_{1-x}Mn_xGeP_2$+MnP samples with different average Mn content x.

TABLE II. Parameters related to the selected magnetic properties obtained for the $Cd_{1-x}Mn_xGeP_2$+MnP samples with different chemical compositions x, including the helical transition temperature T_S, the Curie temperature T_C, the Curie-Weiss temperature θ, the Curie constant C, the active Mn content x_θ calculated from the Curie constant using Eq. (2), the saturation magnetization M_S at 4.5 K, and the active Mn content, x_m.

x	$T_S \pm \Delta T_S$ (K)	$T_C \pm \Delta T_C$ (K)	$C \pm \Delta C (10^{-5})$ (emu K/g)	$x_\theta \pm \Delta x_\theta$	$\theta \pm \Delta\theta$ (K)	$M_S \pm \Delta M_S$ (emu/g)	$x_m \pm \Delta x_m$
0.008 ± 0.001	78 ± 1	295 ± 1	8.8 ± 0.8	0.005 ± 0.001	-227 ± 1	1.4 ± 0.1	0.012 ± 0.001
0.016 ± 0.001	61 ± 1	293 ± 1	9.6 ± 0.9	0.005 ± 0.001	-297 ± 1	1.3 ± 0.1	0.011 ± 0.001
0.023 ± 0.002	56 ± 1	295 ± 1	27 ± 2	0.015 ± 0.001	-346 ± 1	3.0 ± 0.1	0.026 ± 0.002
0.037 ± 0.002	54 ± 1	294 ± 1	33 ± 3	0.019 ± 0.002	-381 ± 1	3.2 ± 0.1	0.027 ± 0.002

with a significant percentage. This effect is coherent with the results of SEM/EDX measurements indicating that the significant percentage of all manganese ions present in our crystals is distributed uniformly in the crystal lattice. Most probably, it is related to the solubility of Mn, higher in II-IV-V_2 group semiconductors, i.e., $Zn_{1-x}Mn_xGeAs_2$ [35] or $Cd_{1-x}Mn_xGeAs_2$ [36], than in their binary counterparts, i.e., III-V semiconductors such as GaP:Mn [34].

Above ~ 50 K, the $Re(\chi_{AC})(T)$ dependencies increase with temperature, which is a signature of a magnetic transition in the samples. Similar behavior was observed for MnP in different forms [31] and in the GaP:MnP system [34], and interpreted as a first order transition between the high-temperature ferromagnetic state and the low-temperature helical phase. In MnP the helical state is related to the competition between magnetic interactions with opposite signs of the exchange constant and strong magnetic anisotropy. As a consequence, in the helical (screw) structure the magnetic moments of Mn ions are confined within the bc crystallographic plane and perform rotation along the a plane. It is therefore evident to assign this transition to the presence of MnP clusters in the $CdGeP_2$ lattice. The temperature of this transition, T_S, defined as a maximum of the derivative of the $Re(\chi_{AC})(T)$ dependence, and listed in Table II, shows large changes as a function of the average Mn contents, i.e., from 78 K for $x = 0.008$ down to 54 K for $x = 0.037$. Large changes of T_S for MnP clusters are known and related to the changes in the size of the inclusions. De Andrés *et al.* showed that the helical phase has $T_S = 47$ K for bulk MnP, 67 K for thin film MnP, and 82 K for MnP nanocrystals [34]. Therefore, it is also possible that the change of T_S observed in our samples is related to the finite-size effect which is associated with the sizes of the inclusions. Above the temperature of about 80 K, the real part of the magnetic susceptibility shows only slight changes up to about 280 K where ferromagnetic-paramagnetic transition is observed.

For the complementation of the AC magnetic susceptibility studies, the DC magnetization measurements were done. For all of the samples, the temperature dependencies of magnetization, $M(T)$, at $B = 500$ mT, from 295 to 600 K were collected (heating regime) and also isothermal magnetic curves, $M(B)$ at selected temperatures. Due to the potential risk of sample annealing during magnetization measurements, resulting in changes of their magnetic properties, we decided to limit the temperature range to $T = 600$ K. It should be noted that the sample holder contribution was subtracted from the experimental results.

The first step in the analysis of the $M(T)$ results was to decide whether the obtained values in the DC and AC studies are consistent. For verification, the DC magnetic susceptibility, namely, χ_{DC}, for each of our $Cd_{1-x}Mn_xGeP_2$+MnP samples was calculated from the $M(T)$ data. The χ_{DC} value obtained at 300 K was comparable to $Re(\chi_{AC})(T = 300$ K); thus these quantities can be used interchangeably. In Fig. 4, the obtained results are presented as the temperature dependencies of the inverse DC magnetic susceptibility, $(\chi_{DC})^{-1}$, together with the lines being the fitted modified Curie-Weiss law [Eq. (1)] to the high-temperature linear (paramagnetic) part of the experimental data. The formula for the modified Curie-Weiss law used for our fitting is given below:

$$\chi_{DC} = \frac{C}{T - \theta} + \chi_{dia}, \qquad (1)$$

where C is the Curie constant, θ is the paramagnetic Curie-Weiss temperature, and χ_{dia} is the diamagnetic susceptibility of the nonmagnetic $CdGeP_2$ host crystal used in fitting as a constant value (the source of it is described further). The Curie constant C is expressed as

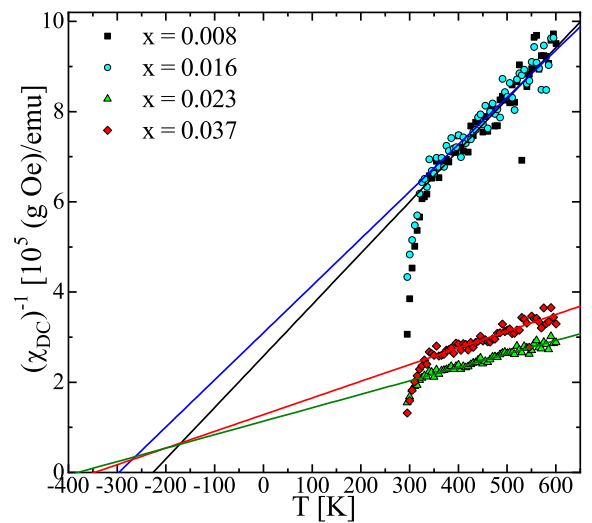$$C = \frac{N_0 g^2 \mu_B^2 J(J+1)x_\theta}{3k_B}, \qquad (2)$$

FIG. 4. Temperature dependencies of the inverse DC magnetic susceptibility collected at $B = 500$ mT for the $Cd_{1-x}Mn_xGeP_2$+MnP samples with different average Mn content x (markers) and fitted Curie-Weiss law to the high-temperature part of the experimental data (lines).
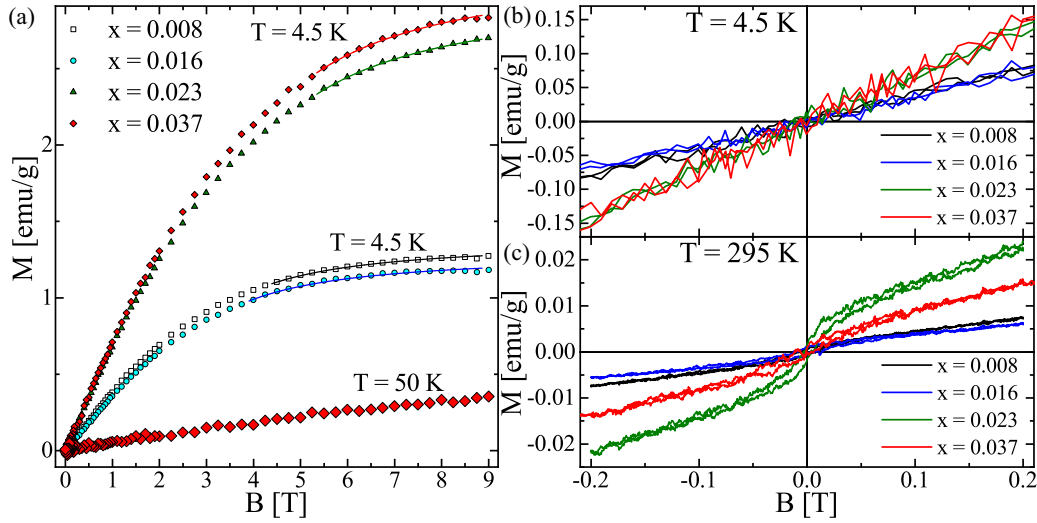
FIG. 5. Selected results of the magnetization measurements (points) obtained for $Cd_{1-x}Mn_xGeP_2+MnP$ samples with different average Mn content x, including magnetization curves (a) measured up to 9 T at $T = 4.5$ K and lines representing fitting the experimental data to different models, and [(b),(c)] in the field range ± 0.2 T at $T = 4.5$ K [top (b)] and $T = 295$ K [bottom (c)].

where N_0 is the number of cation sites per gram, g is the effective spin splitting factor (for Mn ions $g \approx 2$), J is the total magnetic momentum of Mn (for Mn^{2+} in a high-spin state $J = S = 5/2$), x_θ is the content of the magnetically active Mn ions, μ_B is the Bohr magneton, and k_B is the Boltzmann constant. In order to properly take into account the nonzero χ_{dia} value in Eq. (1) during the fitting procedure, the magnetic susceptibility for pure $CdGeP_2$ sample was measured and the χ_{dia} value was estimated as -2×10^{-7} emu/g. It should be highlighted that the values predicted in the literature are quite similar; i.e., for $ZnGeAs_2$ $\chi_{dia} = -2 \times 10^{-7}$ emu/g [35] and for $CdGeAs_2$ $\chi_{dia} = -2.5 \times 10^{-7}$ emu/g [36]. Analyzing the fitting results (presented together with the experimental data in Fig. 4), it should be emphasized that the used modified Curie-Weiss law [Eq. (1)] very well described the experimental data in the entire temperature range above T_C. In Table II we have listed the fitting parameters obtained for all our samples, together with the calculated amount of magnetically active Mn ions, x_θ, by using Eq. (2). For all samples we obtained $x_\theta < x$. It is therefore possible that the charge state of a large fraction of the Mn ions allocated in our $Cd_{1-x}Mn_xGeP_2+MnP$ composites can be different from Mn^{2+}, which is a high-spin state. Another explanation is related to underestimation of the x_θ values during the fitting procedure. For proper application of the Curie-Weiss law we should use the data for $T \gg T_C$, conditions impossible to meet from the point of view of experimental limitations and the potential sample annealing. It is therefore possible that the obtained x_θ values were underestimated.

The Curie-Weiss fitting gave us the values of the Curie-Weiss temperature θ for all our samples, presented in Table II. As we can see, all the obtained Curie-Weiss temperature values are negative, decreasing as a function of the Mn content x. This feature could be a signature of the antiferromagnetic interactions present in our system. From the literature it is known that the complex magnetic structures of MnP can show antiferromagnetism for different Mn-Mn distances [37]. It

is therefore evident, in line with our XRD results showing lack of proper diffraction patterns for MnP clusters, that in samples the MnP clusters show strong internal strain allowing antiferromagnetic interactions to appear.

We studied the magnetic properties of $Cd_{1-x}Mn_xGeP_2+MnP$ composites via measurements of the magnetic field dependence of the magnetization M obtained at several different stabilized constant temperatures. The $M(B)$ relations obtained at different temperatures for $Cd_{1-x}Mn_xGeP_2+MnP$ samples with different chemical compositions are presented in Fig. 5.

For all samples the $M(B)$ curves obtained at $T < T_S$ change significantly with decreasing temperature down to 4.5 K [see exemplary data for $T = 4.5$ and 50 K in Fig. 5(a)]. The magnetization curves measured at $T = 4.5$ K display zero coercivity and do not saturate in the investigated field range. To determine the M_S values, we made several attempts to fit the experimental data to different models describing a field dependence of magnetization. We fitted the experimental data using the Brillouin function for the paramagnet:

$$M = M_S B_S \left(\frac{g\mu_B JB}{k_B T} \right) + \chi_{dia} B, \quad (3)$$

with

$$M_S = x_m N_0 \mu_B g J, \quad (4)$$

where B_S is the Brillouin function and x_m is related to the effective manganese content. Also, we fitted the experimental data to the Brillouin function proposed by the molecular field model by the following equation:

$$M = M_S B_S \left[\frac{g\mu_B J(B + \lambda M)}{k_B T} \right] + \chi_{dia} B, \quad (5)$$

where λ is the molecular field constant. Both models failed due to different reasons. The Brillouin function for the paramagnet does not fit the data well, since at low temperatures the

system potentially consists of magnetically ordered clusters and the paramagnetic host. Fits using Eq. (5) were done by solving numerically for a set of fitting parameter values varied by small amounts in order to inductively get close to the best variance value. The obtained fits reproduce well the experimental data only for negative values of the molecular field constant λ. This in turn suggests that strong antiferromagnetic interactions are present in our samples, an argument in line with the previously observed negative Curie-Weiss temperature values. Since the analysis performed using the Brillouin function indicates the presence of antiferromagnetic interactions, it should be naturally associated with the destruction of the helical phase. It is possible that the MnP clusters due to their strain or size effects are forming an incommensurate magnetic structure, which gives rise to antiferromagnetic spin waves to be dominant.

A proper Brillouin function fit for the antiferromagnetic system requires introduction of two independent molecular field constants related to the inter- and the intrasublattice interactions. Such analysis cannot be reliably done due to too many fit parameters. To make the saturation magnetization values credible we applied a third approach, in which we fitted the high-field part of the experimental data with the phenomenological scaling approach law [38] given by the following equation:

$$M = M_S \left(1 - \frac{a_1}{B} - \frac{a_2}{B^2} \right) + \chi_{\text{dia}} B, \qquad (6)$$

where a_1 and a_2 are phenomenological constants. We fitted the experimental results obtained at $T = 4.5$ K with constant contribution of the lattice diamagnetism, $\chi_{\text{dia}} = -3 \times 10^{-7}$ emu/(g Oe) (value estimated during dynamic magnetic susceptibility measurements), and obtained M_S values similar to that found for the other II-IV-V_2 semiconductors [35,36]. The M_S values obtained in the third model are listed for all of our samples in Table II. As we can see M_S is, in most cases, an increasing function of the average Mn content x.

From Eq. (4) we can estimate the values of the effective Mn content x_{m}. The obtained values are listed in Table II. The comparison between the x_{m} and x_θ shows that for all samples $x_{\text{m}} > x_\theta$. It is a signature that the x_θ values obtained during the analysis of the $\chi_{\text{DC}}(T)$ curves based on the modified Curie-Weiss law were underestimated. It is probably related to the too narrow temperature range (in relation to the Curie temperature) in the Curie-Weiss fitting. Therefore, the values of x_{m} should be treated as better reflecting the actual amount of Mn in the samples. The obtained x_{m} values are different than x. For the samples with $x = 0.008$ and $x = 0.016$, even taking into account errors in x and x_{m} values, the x_{m} value is only slightly ($\Delta x = 0.001$) larger than x. It should be also noted that the net magnetic moment for MnP equals about $1.29 \, \mu_B$ [37], a value slightly larger than our assumption and explaining the observed $x_{\text{m}} > x$. It is therefore reasonable to assume that for the samples with $x = 0.008$ and 0.023 a majority of Mn ions were in a Mn^{2+} high-spin state with $J = S = 5/2$. In contrast to the above two samples, for the samples with $x = 0.016$ and 0.037 the obtained x_{m} is about 37%–45% smaller than x indicating that a large fraction of Mn ions is having a smaller net magnetic moment per ion. This situation is well described within the theoretical approach

presented in Ref. [37], where the effect of local strain on the net magnetic moment of the Mn ion in MnP is discussed. It is therefore evident that our findings are in line with this interpretation. We believe that for the two samples in which $x_{\text{m}} < x$ it is due to strain-driven moment reduction.

The magnetization curves observed at 4.5 K indicate that the properties of MnP clusters are similar to those for MnP single crystals and are caused by magnetic anisotropy effects. In particular, the $M(B)$ curves obtained at $T = 4.5$ K do not show saturation due to the magnetocrystalline anisotropy of the MnP clusters with a hard magnetic axis (a axis) parallel with respect to the external magnetic field [34]. Such behavior is pronounced for the samples with the largest x ($x = 0.023$ and $x = 0.037$). The $M(B)$ curves for the samples with $x = 0.008$ and $x = 0.023$ show a trend towards saturation suggesting that the MnP clusters are oriented with respect to the magnetic field along the magnetic b axis (believed to be the intermediate direction of magnetization [33]).

Attention should also be paid to the magnetic state at 4.5 K. At temperature $T < T_S$, the coercive field H_C and remnant magnetization M_R, estimated based on the magnetization curves, show nearly zero values for all samples. As mentioned earlier, below T_S our samples are in the helical (screw) state. Magnetization curves with nonzero coercive field were observed well below $T = 50$ K in the MnP films and in MnP clusters embedded in GaP [34]. The absence of a coercive field occurs in a powder MnP sample [34], or in single crystals [31,32]. As reported by Huber and Ridgley in Ref. [32], the helical phase below 50 K for the MnP single crystal is the metamagnetic state. It means that within this state both antiferromagnetic and ferromagnetic interactions are present. In a similar case, a steplike $M(B)$ field dependence should be observed, with a coercivity close to zero. It is therefore probable, in agreement with our SEM/EDS data, that the MnP clusters in our samples do not have the form of single crystals, but are built of conglomerated MnP polycrystalline powder.

Both the a and b axes show complex magnetic states below 50 K. These helical phases are known as fan, cone, and screw states. Thus, observation of Brillouin-like behavior of the $M(B)$ curves is associated with the field-induced transition from screw to fan phase (along axis b) or screw to cone to fan (along axis a), as it follows from the magnetic phase diagram of MnP single crystals [31,34].

At higher temperatures in the range $T_S < T < T_C$, a small coercive field is present in all our samples. The coercive field becomes visible (higher than the uncertainty of the magnetic field in the superconducting magnet equal to about 5 G) at about 75 K, and shows only a small decrease with temperature up to T_C. At $T > T_C$ the coercive field is small and changes from about 60 G for the sample with $x = 0.008$ down to about 20 G for the sample with $x = 0.037$. It is a signature of the magnetic coupling of magnetic ions in the MnP clusters present in the material.

V. COMPARISON BETWEEN DOPING AND PRESSURE EFFECT

To understand the relationship between magnetic and structural behavior in the investigated compounds, it will be useful to establish the influence of Mn doping and external
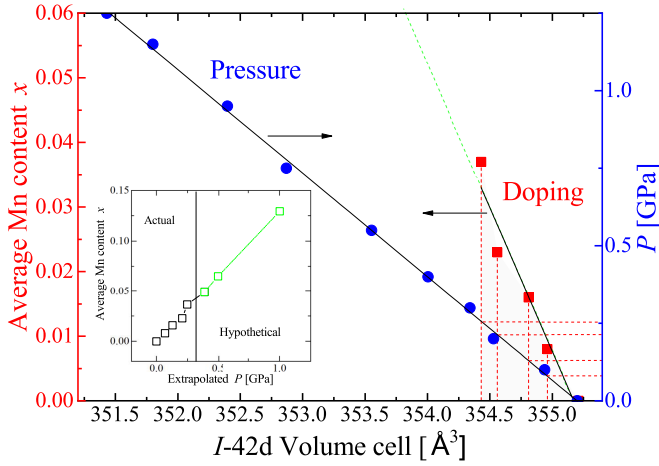
FIG. 6. Comparison between Mn doping and pressure effect, plotted against the CdGeP$_2$ volume cell. Solid lines indicate the linear fitting of both dependences. The red dashed lines show extrapolation from the point of Mn doping to linear dependence with P. The obtained extrapolated pressure data are plotted against the average Mn content, as shown in the inset. Green dashed lines correspond to hypothetical continuation of the $x(P)$ dependence.

FIG. 7. *T-P* magnetic phase diagram of Cd$_{1-x}$Mn$_x$GeP$_2$+MnP, including magnetic transitions T_C and T_S from Table II, compared with the same transitions in bulk MnP from Refs. [25,39,40]. Dashed lines correspond to hypothetical continuation of the $T_C(P)$ and $T_S(P)$ dependencies. FM denotes the ferromagnetic, SCR denotes the helical (screw), and PM denotes the paramagnetic state.

pressure P on the magnetic properties of bulk CdGeP$_2$. Since the presence of the additional Ge phase for $x > 0$ in the composite is not significant (less than ∼10%) as it follows from our HRXRD measurements, we believe that Mn doping is associated with the chalcopyrite phase (I-$42d$). Figure 6 shows the combined dependence of the average Mn content and external pressure from the volume of the chalcopyrite unit cell. The high-pressure volumetric measurements up to 5 GPa were performed in a toroid-type pressure cell under hydrostatic conditions [24]. The actual values of x and the corresponding volume lattice parameters are from Table I, while the P-V data for CdGeP$_2$ are extracted from volumetric measurements in Ref. [24]. As can be seen, these values do not scale to each other, since pressure has a stronger effect on the change in the volume cell. However, by subtracting from the overall volumetric data the line related to the Mn doping and to the linear dependence of P allows one to estimate the effect of "local" pressure, which is due to the complete incorporation of Mn.

The value of the local pressure equal to $P \sim 0.25$ GPa corresponds to the ultimate content $x = 0.035$ in the samples, as shown in the inset to Fig. 6. Assuming the ratio between the actual average Mn content and P remains directly proportional, to achieve a local pressure of about 1 GPa, a significant excess in $x \sim 0.135$ will be required (green dashed line in Fig. 6 and in the inset).

Also, we have constructed a *T-P* phase diagram using the values of T_C and T_S (Table II) as a function of the extrapolated pressure (doping) up to 1 GPa that includes both actual doping concentrations of $x = 0.008$ to 0.035 and their hypothetical continuation (Fig. 7). For comparison, the phase diagram shows the temperatures of magnetic transitions for bulk MnP under hydrostatic compression [25,39,40]. The obtained phase diagram at first glance demonstrates a certain analogy between bulk MnP and MnP clusters. However, it can
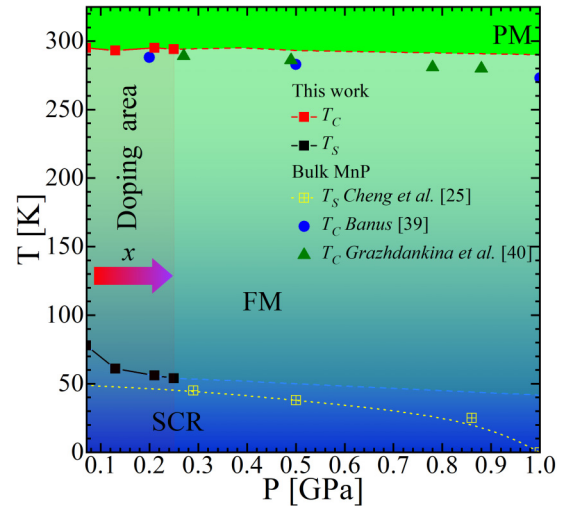
be seen that T_C for clusters remains nearly constant, while T_S shows a monotonic decrease from 78 to 54 K within the pressure window up to 1 GPa. In the next section, we will discuss possible physical mechanisms responsible for this behavior.

VI. DISCUSSION

From the results of the magnetic measurements performed with the use of three different magnetometric methods, it is argued that the origin of magnetic transitions in Mn-doped CdGeP$_2$ is associated with the micron-size MnP clusters. The magnetic transition related to the MnP clusters even for $x < 0.016$ lying below the solubility limit of Mn ($x \approx 0.01$) in the matrix is well visible in the Re(χ_{AC})(T) dependence (Fig. 3). The contribution from magnetic clusters is dominant in the entire group of materials II-IV-V$_2$ and is responsible for the ferromagnetism observed at room temperature [14]. As reported by Cho *et al.* [12], the changes of slope in the temperature dependence of the resistance at around 47 and 312 K in (Zn$_{1-x}$Mn$_x$)GeP$_2$ are obviously a consequence of the presence of MnP clusters, which, as in this study, cannot be detected using XRD characterization. A similar conclusion was argued by Hwang *et al.* [41], who have explained this inconsistency by the weak crystallinity of the MnP phase.

Aside from the cogent fact of the MnP clusters' predominance, a question related to the random distribution of Mn in the composite still remains unsolved. The conventional mechanism of Mn substitution in the CdGeP$_2$ lattice is related to the creation of intrinsic defects, which for the most part are cation vacancies at Cd sites and vacancies at Ge sites. [13]. Since an additional Ge ($Fd3m$) cubic phase is identified for the samples with $x > 0$, it may indicate that the Ge vacancy in the chalcopyrite lattice is actively involved in the substitution mechanism; i.e., the formation of a separate Ge phase most likely arises from the compensation of the Mn excess. As follows from Table I, the unit cell volume V_1 gradually

decreases with increasing x, which is unexpected. This is due to the mechanism that arises when the solubility limit is surpassed; the change in V_1 should remain near a constant value. Simultaneously, the lattice parameter a_2 shows an increase from 5.6240(2) to 5.65778(5) Å for $x = 0$ and $x = 0.016$, respectively, and no longer changes for $x > 0.016$. It can be assumed that the excess Mn is redistributed in some way onto the cubic Ge structure, and an increase in a_2 occurs due to the difference in ionic radii between Mn and Ge. However, there is no evidence coming from our magnetic measurements that indicate any magnetic transitions associated with MnGe precipitates [42]. Then, a decrease in V_1 can be understood by substitution of Mn in both the cationic sites, i.e., Cd and Ge [13].

Next, based on the T-P phase diagram (Fig. 7), we discuss the behavior of T_C and T_S for MnP clusters in comparison to bulk MnP as a function of local pressure (doping). A characteristic property of bulk MnP is that both magnetic transition temperatures decrease with increasing P. As shown by Banus [39], bulk T_C has a strong shift at a rate of about -18.5 K/GPa up to 2 GPa, and further between 2 and 3 GPa the slope changes to -25 K/GPa. A similar decrease in T_C is also confirmed by Grazhdankina *et al.* [40] from magnetotransport measurements up to ~ 1.2 GPa. In parallel, at the low-temperature region, the helical phase with a transition temperature around $T_S \sim 50$ K at ambient pressure decreases with increasing pressure and completely disappears at 1.2 GPa [25]. Ferromagnetism, however, still exists below $T_C = 250$ K, and then transforms into a conical or two-phase (ferromagnetic and spiral) state below 150 K, and entirely disappears at 3.8 GPa. At 3.8 GPa, only a spiral structure is observed, which retains up to 8 GPa, where superconductivity emerges [25,26]. Tantamount to the effect of high pressure, doping by $3d$ elements of the orthorhombic MnP structure induces similar changes. In Co-substituted MnP, an increase in the concentration up to 5% significantly reduces T_C to 240 K and the helimagnetic (screw) phase is no longer observed, which is explained in terms of the topological Hall effect modified by the Dzyaloshinsky-Moriya interaction [43]. With respect to MnP clusters, the behavior of magnetic transitions, in particular at T_C, cannot be unambiguously interpreted from the standpoint of hydrostatic (Fig. 7) and even uniaxial compression applied along different crystallographic directions [44]. As shown for the MnP nanocrystals embedded in GaP [34,45], as well as in our case, T_C remains near a constant value close to 291 K, while T_S varies in a manner similar to the changes as a function of the applied pressure. An attempt to find an acceptable explanation for such behavior naturally should be related to the finite-size and surface effects of the clusters due to the restraining medium (matrix).

We conclude that an important difference between the $Cd_{1-x}Mn_xGeP_2$+MnP composite and MnP nanocrystals embedded in GaP or even MnP thin films lies in a gradual decrease in the volume of the host lattice due to the local pressure effect. Meanwhile, the MnP clusters are strongly coupled with the chalcopyrite structure, and as it has been found they modified the magnetic transition temperatures. In particular, T_S compared to T_C turns out to be more sensitive due to the possible contribution from the thermal expansion through the coupled $CdGeP_2$ structure at decreasing T. We also note that the magnetic interactions from randomly distributed Mn ions in the matrix cannot be the cause of the observed changes in T_C and T_S, since their paramagnetic contribution is observed at very low temperatures ($T \ll 50$ K).

VII. SUMMARY

In conclusion, on the basis of structural and magnetic measurements of the $Cd_{1-x}Mn_xGeP_2$ composite with $0 \leqslant x \leqslant 0.037$, we have confirmed that the presence of micronsized MnP (10–30 μm) clusters is the dominant source of the observed magnetic interactions in this material. Along with MnP clusters, the randomly distributed Mn ions within a chalcopyrite structure, whose charge state is rather different from Mn^{2+}, indicate a notable paramagnetic response on the background of the low-temperature helical (screw) phase. Moreover, the analysis of the low-temperature magnetization performed by the Brillouin function and the negative Curie-Weiss temperature suggest for antiferromagneticlike interaction, which is most likely associated with the destruction of the helical structure due to enhanced strain effects of MnP clusters.

The origin of the observed magnetic transitions at T_C and T_S is characterized by similarity to bulk MnP. The quantitative difference is only that $T_C \sim 295$ K remains near a constant value when T_S decreases from 78 to 54 K in the limit of $x = 0.008$ to 0.037. The discussed reason for this behavior is connected with the idea of a local pressure arising in the $CdGeP_2$ lattice, at which the maximum value of $P \sim 0.25$ GPa corresponds to the ultimate content $x = 0.035$ used in this work. The formation of MnP clusters whose signatures appear well below the limit of Mn solubility in the chalcopyrite lattice ($x \approx 0.01$), is a fundamental property of most of the phosphorus-containing magnetic chalcopyrites [12,22].

[1] J. Kossut and W. Dobrowolski, *Handbook of Magnetic Materials* (North-Holland, Amsterdam, 1993), pp. 231–305.

[2] W. Dobrowolski, J. Kossut, and T. Story, *Handbook of Magnetic Materials* (Elsevier, Amsterdam, 2003), Chaps. II–VI, pp. 289–377.

[3] T. Dietl, A ten-year perspective on dilute magnetic semiconductors and oxides, Nat. Mater. **9**, 965 (2010).

[4] T. Dietl and H. Ohno, Dilute ferromagnetic semiconductors: Physics and spintronic structures, Rev. Mod. Phys. **86**, 187 (2014).

[5] M. Wang, R. P. Campion, A. W. Rushforth, K. W. Edmonds, C. T. Foxon, and B. L. Gallagher, Achieving high Curie temperature in (Ga,Mn)As, Appl. Phys. Lett. **93**, 132103 (2008).

[6] V. Novák, K. Olejník, J. Wunderlich, M. Cukr, K. Výborný, A. W. Rushforth, K. W. Edmonds, R. P. Campion, B. L. Gallagher, J. Sinova, and T. Jungwirth, Curie Point Singularity in the Temperature Derivative of Resistivity in (Ga,Mn)As, Phys. Rev. Lett. **101**, 077201 (2008).

[7] L. Chen, S. Yan, P. F. Xu, J. Lu, W. Z. Wang, J. J. Deng, X. Qian, Y. Ji, and J. H. Zhao, Low-temperature magnetotransport behaviors of heavily Mn-doped (Ga,Mn)As films with high ferromagnetic transition temperature, Appl. Phys. Lett. **95**, 182505 (2009).

[8] K. Khazen, H. J. von Bardeleben, J. L. Cantin, A. Mauger, L. Chen, and J. H. Zhao, Intrinsically limited critical temperatures of highly doped $Ga_{1-x}Mn_x$As thin films, Phys. Rev. B **81**, 235201 (2010).

[9] P. Němec, V. Novák, N. Tesařová, E. Rozkotová, H. Reichlová, D. Butkovičová, F. Trojánek, K. Olejník, P. Malý, R. P. Campion, B. L. Gallagher, J. Sinova, and T. Jungwirth, The essential role of carefully optimized synthesis for elucidating intrinsic material properties of (Ga,Mn)As, Nat. Commun. **4**, 1422 (2012).

[10] M. Wang, K. W. Edmonds, B. L. Gallagher, A. W. Rushforth, O. Makarovsky, A. Patanè, R. P. Campion, C. T. Foxon, V. Novák, and T. Jungwirth, High Curie temperatures at low compensation in the ferromagnetic semiconductor (Ga,Mn)As, Phys. Rev. B **87**, 121301(R) (2013).

[11] Y.-J. Zhao, W. T. Geng, A. J. Freeman, and T. Oguchi, Magnetism of chalcopyrite semiconductors: $Cd_{1-x}Mn_x$GeP$_2$, Phys. Rev. B **63**, 201202(R) (2001).

[12] S. Cho, S. Choi, G.-B. Cha, S. Ch. Hong, Y. Kim, Y.-J. Zhao, A. J. Freeman, J. B. Ketterson, B. J. Kim, Y. C. Kim, and B.-Ch. Choi, Room-Temperature Ferromagnetism in ($Zn_{1-x}Mn_x$)GeP$_2$ Semiconductors, Phys. Rev. Lett. **88**, 257203 (2002).

[13] P. Mahadevan and A. Zunger, Room-Temperature Ferromagnetism in Mn-Doped Semiconducting CdGeP$_2$, Phys. Rev. Lett. **88**, 047205 (2002).

[14] S. C. Erwin and I. Žutić, Tailoring ferromagnetic chalcopyrites, Nat. Mater. **3**, 410 (2004).

[15] V. M. Novotortsev, A. V. Kochura, and S. F. Marenkin, New ferromagnetics based on manganese-alloyed chalcopyrites $A^{II}B^{IV}C^{V}_2$, Inorg. Mater. **46**, 1421 (2010).

[16] L. Kilanski, M. Górska, W. Dobrowolski, E. Dynowska, M. Wójcik, B. J. Kowalski, J. R. Anderson, C. R. Rotundu, D. K. Maude, S. A. Varnavskiy, I. V. Fedorchenko, and S. F. Marenkin, Magnetism and magnetotransport of strongly disordered $Zn_{1-x}Mn_x$GeAs$_2$ semiconductor: The role of nanoscale magnetic clusters, J. Appl. Phys. **108**, 073925 (2010).

[17] L. Kilanski, W. Dobrowolski, E. Dynowska, M. Wójcik, B. J. Kowalski, N. Nedelko, A. Ślawska-Waniewska, D. K. Maude, S. A. Varnavskiy, I. V. Fedorchenko, and S. F. Marenkin, Colossal linear magnetoresistance in a CdGeAs$_2$:MnAs microcomposite ferromagnet, Solid State Commun. **151**, 870 (2011).

[18] I. V. Fedorchenko, L. Kilanski, I. Zakharchuk, P. Geydt, E. Lahderanta, P. N. Vasilyev, N. P. Simonenko, A. N. Aronov, W. Dobrowolski, and S. F. Marenkin, Composites based on self-assembled MnAs ferromagnet nanoclusters embedded in ZnSnAs$_2$ semiconductor, J. Alloys Compd. **650**, 277 (2015).

[19] L. Kilanski, I. V. Fedorchenko, M. Górska, A. Ślawska-Waniewska, N. Nedelko, A. Podgórni, A. Avdonin, E. Lahderanta, W. Dobrowolski, A. N. Aronov, and S. F. Marenkin, Magnetoresistance control in granular $Zn_{1-x-y}Cd_xMn_y$GeAs$_2$ nanocomposite ferromagnetic semiconductors, J. Appl. Phys. **118**, 103906 (2015).

[20] T. R. Arslanov, R. K. Arslanov, L. Kilanski, T. Chatterji, I. V. Fedorchenko, R. M. Emirov, and A. I. Ril, Low-field-enhanced unusual hysteresis produced by metamagnetism of the MnP clusters in the insulating CdGeP$_2$ matrix under pressure, Phys. Rev. B **94**, 184427 (2016).

[21] T. R. Arslanov, L. Kilanski, S. López-Moreno, A. Yu. Mollaev, R. K. Arslanov, I. V. Fedorchenko, T. Chatterji, S. F. Marenkin, and R. M. Emirov, Changes in the magnetization hysteresis direction and structure-driven magnetoresistance of a chalcopyrite-based magnetic semiconductor, J. Phys. D: Appl. Phys. **49**, 125007 (2016).

[22] G. A. Medvedkin, T. Ishibashi, T. Nishi, K. Hayata, Y. Hasegawa, and K. Sato, Room temperature ferromagnetism in novel diluted magnetic semiconductor $Cd_{1-x}Mn_x$GeP$_2$, Jpn. J. Appl. Phys. **39**, L949 (2000).

[23] C. C. Becerra, Y. Shapira, N. F. Oliveira, Jr., and T. S. Chang, Lifshitz Point in MnP, Phys. Rev. Lett. **44**, 1692 (1980).

[24] T. R. Arslanov, A. Yu. Mollaev, I. K. Kamilov, R. K. Arslanov, L. Kilanski, R. Minikaev, A. Reszka, S. López-Moreno, A. H. Romero, M. Ramzan, P. Panigrahi, R. Ahuja, V. M. Trukhan, T. Chatterji, S. F. Marenkin, and T. V. Shoukavaya, Pressure control of magnetic clusters in strongly inhomogeneous ferromagnetic chalcopyrites, Sci. Rep. **5**, 7720 (2015).

[25] J.-G. Cheng, K. Matsubayashi, W. Wu, J. P. Sun, F. K. Lin, J. L. Luo, and Y. Uwatoko, Pressure Induced Superconductivity on the Border of Magnetic Order in MnP, Phys. Rev. Lett. **114**, 117001 (2015).

[26] M. Matsuda, F. Ye, S. E. Dissanayake, J.-G. Cheng, S. Chi, J. Ma, H. D. Zhou, J.-Q. Yan, S. Kasamatsu, O. Sugino, T. Kato, K. Matsubayashi, T. Okada, and Y. Uwatoko, Pressure dependence of the magnetic ground states in MnP, Phys. Rev. B **93**, 100405(R) (2016).

[27] J. A. Aitken, G. M. Tsoi, L. E. Wenger, and S. L. Brock, Phase segregation of MnP in chalcopyrite dilute magnetic semiconductors: A cautionary tale, Chem. Mater. **19**, 5272 (2007).

[28] K. Sato, G. A. Medvedkin, T. Ishibashi, S. Mitani, K. Takanashi, Y. Ishida, D. D. Sarma, J. Okabayashi, A. Fujimori, T. Kamatani, and H. Akai, Novel Mn-doped chalcopyrites, J. Phys. Chem. Solids **64**, 1461 (2003).

[29] V. M. Novotortsev, S. A. Varnavskii, S. F. Marenkin, L. I. Koroleva, R. V. Demin, V. M. Trukhan, S. O. Klimonskii, and V. D. Kuznetsov, Ferromagnetic material CdGeP$_2$:Mn for spintronics, Russ. J. Inorg. Chem. **51**, 1153 (2006).

[30] A. Zieba, C. C. Becerra, H. Fjellvag, N. F. Oliveira, and A. Kjekshus, $Mn_{0.9}Co_{0.1}$P in an external field: Lifshitz point and irreversibility behavior of disordered incommensurate phases, Phys. Rev. B **46**, 3380 (1992).

[31] M. S. Reis, R. M. Rubinger, N. A. Sobolev, M. A. Valente, K. Yamada, K. Sato, Y. Todate, A. Bouravleuv, P. J. von Ranke, and S. Gama, Influence of the strong magnetocrystalline anisotropy on the magnetocaloric properties of MnP single crystal, Phys. Rev. B **77**, 104439 (2008).

[32] E. E. Huber and D. H. Ridgley, Magnetic properties of a single crystal of manganese phosphide, Phys. Rev. **135**, A1033 (1964).

[33] T. Komatsubara, H. Shinohara, T. Suzuki, and E. Hirahara, Spin structure as a function of magnetic field and temperature in MnP single crystal, J. Appl. Phys. **40**, 1037 (1969).

[34] A. de Andrés, A. Espinosa, C. Prieto, M. García-Hernández, R. Ramírez-Jiménez, S. Lambert-Milot, and R. A. Masut, MnP films and MnP nanocrystals embedded in GaP epilayers grown on GaP(001): Magnetic properties and local bonding structure, J. Appl. Phys. **109**, 113910 (2011).

[35] L. Kilanski, K. Szałowski, R. Szymczak, M. Górska, E. Dynowska, P. Aleshkevych, A. Podgórni, A. Avdonin, W. Dobrowolski, I. V. Fedorchenko, and S. F. Marenkin, Low-dilution limit of $Zn_{1-x}Mn_xGeAs_2$: Electrical and magnetic properties, J. Appl. Phys. **114**, 093908 (2013).

[36] L. Kilanski, M. Górska, E. Dynowska, A. Podgórni, A. Avdonin, W. Dobrowolski, I. V. Fedorchenko, and S. F. Marenkin, Homogeneous limit of $Cd_{1-x}Mn_xGeAs_2$ alloy: Electrical and magnetic properties, J. Appl. Phys. **115**, 133917 (2014).

[37] Z. Gercsi and K. G. Sandeman, Structurally driven metamagnetism in MnP and related *Pnma* compounds, Phys. Rev. B **81**, 224426 (2010).

[38] A. Aharoni, One-dimensional theory of the parasitic paramagnetism term in the approach to saturation, Phys. Rev. **132**, 105 (1963).

[39] M. D. Banus, Effect of pressures to 50 kbar on the magnetic behavior of MnP, J. Solid State Chem. **4**, 391 (1972).

[40] N. P. Grazhdankina, A. M. Burkhanov, and Y. S. Bersenev, The effect of hydrostatic pressure on the Curie temperature of manganese monophosphide, Zh. Eksp. Teor. Fiz. **55**, 2155 (1968) [Sov. Phys. JETP **28**, 1141 (1969)].

[41] T. Hwang, J. H. Shim, and S. Lee, Observation of MnP magnetic clusters in room-temperature ferromagnetic semiconductor $Zn_{1-x}Mn_xGeP_2$ using nuclear magnetic resonance, Appl. Phys. Lett. **83**, 1809 (2003).

[42] T. Devillers, M. Jamet, A. Barski, V. Poydenot, P. Bayle-Guillemaud, E. Bellet-Amalric, S. Cherifi, and J. Cibert, Structure and magnetism of self-organized $Ge_{1-x}Mn_x$ nanocolumns on Ge(001), Phys. Rev. B **76**, 205306 (2007).

[43] Y. Shiomi, S. Iguchi, and Y. Tokura, Emergence of topological Hall effect from fanlike spin structure as modified by Dzyaloshinsky-Moriya interaction in MnP, Phys. Rev. B **86**, 180404(R) (2012).

[44] E. Hirahara, T. Suzuki, and Y. Matsumura, Effect of pressure on magnetic interactions in metamagnetic MnP Single crystals, J. Appl. Phys. **39**, 713 (1968).

[45] A. de Andrés, R. Ramírez-Jiménez, M. García-Hernández, S. Lambert-Milot, and R. A. Masut, Confinement effects on the low temperature magnetic structure of MnP nanocrystals, Appl. Phys. Lett. **99**, 182506 (2011).